Available online at www.sciencedirect.com
ScienceDirect
Journal of Molecular Catalysis A: Chemical 260 (2006) 269–279
JOURNAL OF MOLECULAR CATALYSIS A: CHEMICAL
www.elsevier.com/locate/molcata

Liquid-phase hydrogenation of methyl oleate on a Ni/α-Al_2O_3 catalyst: A study based on kinetic models describing extreme and intermediate adsorption regimes

Maria I. Cabrera [1], Ricardo J. Grau [*,1]

INTEC, Institute de Desarrollo Tecnologico para la Industria Quimica. Universidad Nacional del Literal (U.N.L.) and Consejo Nacional de Investigaciones Cientificas y Tecnicas (CONICET), Giiemes 3450, (3000) Santa Fe, Argentina

Received 20 June 2006; received in revised form 13 July 2006; accepted 14 July 2006
Available online 1 September 2006

Abstract

The kinetics of the hydrogenation of methyl oleate on a Ni/α-Al_2O_3 catalyst was studied in the absence of mass-transport limitation, at $398 \leq T \leq 443$ K and $3.7 \leq P_{H_2} \leq 6.5$ bar. The kinetic modeling was performed on the basis of elementary step mechanisms involving different regimes of competition between hydrogen and methyl oleate. Admitting a distinction between occupied-sites and covered-sites by the large molecule of methyl oleate, a rigorous proposal was made to link the seemingly separate kinetic models corresponding to the extreme modes of competitive and non-competitive adsorption, without having to draw the common distinction between two types of surface sites. General rate equations were formulated without expressing opinion *a priori* on whether the adsorption regime is competitive or non-competitive. Then, typical LHHW rate equations for both extreme adsorption regimes were straightforwardly derived as special cases. Statistical results demonstrated the inadequacy of the models approaching non-competitive adsorption to describe the experimental data but results did not allow a definite discrimination between rival models with competitive and semi-competitive adsorption. A mechanistic model featuring dissociative adsorption of hydrogen, molecule of methyl oleate interacting with a single atom of Ni, and second insertion of hydrogen as RDS, proved to be the best candidate to describe the experimental data satisfactorily with physically reasonable parameters. As a distinctive feature, the model considering semi-competitive adsorption gave additional indication that the adsorbed molecule of methyl oleate could cover up to seven surface sites. From this finding, the semi-competitive model seems to be more realistic than the competitive one.

Keywords: Hydrogenation; Methyl oleate; Kinetic models; Competitive adsorption; Semi-competitive adsorption; Non-competitive adsorption

1. Introduction

Hydrogenation of fatty oils (FOs) and fatty acid methyl esters (FAMEs) is one of the most important processes in edible oil and oleochemical industries [1,2]. Since its development in the early 1900s, the hydrogenation process has been performed to improve the flavor stability and melting properties of edible oils [3,4]. FAMEs are commonly used as model compounds for the much more complex triglycerides that are found in edible fats and oils. Although nickel-based catalysts isomerize the naturally occurring *cis* double bonds to the undesirable *trans* configurations having adverse health implications, they are still the most commonly used catalysts due to their lower cost compared to other catalysts, e.g., the *cis*-selective palladium [5]. Interest in finding non-edible uses for these renewable sources has increased in recent years due to their growing availability and environment compatibility. Indeed, it is well known that polyunsaturated vegetable oils used as environmentally friendly lubricants and fuel alternatives must also be improved toward oxidation and NO_x emission by selective hydrogenation [6,7].

Considerable work has been done to understand the FOs and FAMEs hydrogenation process with an interest to developing improved hydrogenation technologies. However, the kinetic modeling of the hydrogenation process is still not entirely accomplished due to the complexity arising from the simultaneous adsorption, reduction, migration and geometric isomer-

* Corresponding author. Fax: +54 342 4511079.
E-mail address: cqfina@ceride.gov.ar (R.J. Grau).
[1] Professor at U.N.L. and Member of CONICET's Research Staff.

1381-1169/$ – see front matter © 2006 Elsevier B.V. All rights reserved.
doi:10.1016/j.molcata.2006.07.042

ization of double bonds, which usually take place in the presence of mass transport limitations [3,8–11]. Since the 1970s, the kinetic modeling of this three-phase hydrogenation system has been mainly performed in the mathematical framework of the Langmuir–Hinshelwood–Hougen–Watson (LHHW) formalism. Langmuirian adsorption and rate-limiting reaction step in the adsorbed state are two of the basic assumptions for deriving the classical LHHW rate equations. Mechanistic considerations on whether the species adsorption is competitive or non-competitive, and the hydrogen adsorption is dissociative or non-dissociative are the most debatable underlying assumptions. There are also different conjectures concerning the nature of the active sites. Two types of adsorption sites are necessarily postulated to derive the hydrogenation rate equations describing the non-competitive adsorption mode. Although the Ni-support interactions seem to be playing an important role in the catalytic activity [4,12], the distinction of two types of sites for FAMEs and hydrogen adsorption would be pure speculation if the double bonds are likely chemisorbed on the metal surface involving 2σ- or π-complexes [3,13]. Therefore, it would be ambiguous to assume that FAMEs adsorb at one type of sites and hydrogen adsorbs independently at a second type. Another oversimplified reasoning consists of setting two uncoupled site balances for both the hydrogen and FAMEs at the surface after claiming that the much smaller hydrogen atoms most likely adsorb on sites remaining unoccupied by the large molecules of FAMEs. Likewise, the real adsorption regime of the species could be between the competitive and non-competitive adsorption cases, which are certainly extreme. In this regard, semi-competitive adsorption models have been proposed for the xylosa liquid-phase hydrogenations [14], and *o*-xylene gas-phase hydrogenation [15].

We noticed the lack of kinetic models able to describe intermediate (semi-competitive) competition regimes, which would be present during the hydrogenation of FAMEs. Therefore, the present contribution attempts to match the two seemingly separate kinetic models arising from the competitive and non-competitive adsorption modes, without having to draw the common distinction between two types of surface sites. A workable way to survey semi-competitive adsorption regimes consequently arises. To illustrate the usefulness of the proposed approach, we decided upon the kinetic modeling of the methyl oleate hydrogenation over a Ni/α-Al_2O_3 catalyst in a slurry semi-batch reactor because it is the more simple subsystem of the reaction network describing the hydrogenation of polyunsaturated FAMEs. Rigorous kinetic modeling should include migration of double bonds and *cis–trans* isomerization [3,4,10,16–18]. However, we considered non-distinguishable migration products because the double bond migrates merely only one position along the carbon chain [10], the methyl oleate (*cis*) and methyl elaidate (*trans*) as a lumped species, i.e., without *cis–trans* distinction. We adopted this oversimplified description using the lowest number of adjustable parameters to give an agreeable fit to our experimental data and to facilitate the presentation since further extensions to more complex hydrogenation systems are straightforward.

2. Experimental

2.1. Catalyst and chemicals

A 25 wt% Ni/α-Al_2O_3 catalyst (BET specific surface area 185 m^2/g, mean particle diameter 2.5 μm, mean pore diameter 8 nm) was used in the hydrogenation experiments. The catalyst was conditioned in situ according to a previously reported procedure [19]. Methyl oleate (purity > 98%) was isolated from technical grade methyl oleate (Aldrich, 70%) by high-vacuum distillation. Nitrogen gas (AgaGas, 99.999% pure) and hydrogen gas (AgaGas, 99.999% pure) were flowed through a Deoxo unit and a drying column before use.

2.2. Apparatus and operating conditions

The experimental setup is schematically shown in Fig. 1. All hydrogenation experiments were performed in a stirred three-phase slurry reactor (Parr Instruments Co. Model 4842). The reactor temperature was controlled within ±0.5 K using a system of both electrical heating and coolant circulation to achieve a fast dynamic control of the temperature. The pressure was measured with a strain-gauge pressure transducer (Ashcroft, Model K2) and maintained within ±0.05 bar with a pressure controller (Cole Parmer, Model 68502-10). Hydrogen flow was monitored with a mass flow meter (Matheson 8110).

The temperature was 398, 413 and 443 K, whereas the hydrogen pressure was kept constant at 3.7, 5.1 and 6.5 bar, at each temperature. The catalyst loading was 0.2 wt% with respect to methyl oleate, and the stirring rate was 1000 rpm to ensure that neither gas–liquid nor liquid–solid mass transfer rates affect the reaction rate as analyzed below. Since the kinetic study demands zero induction times, constant catalytic activity and good reproducibility, a cup-and-cap (CAC) device was used to fulfill all these requirements as in our previous studies of the liquid-phase hydrogenation of FAMEs [17,20–23]. The reproducibility of the experimental data was ±1%.

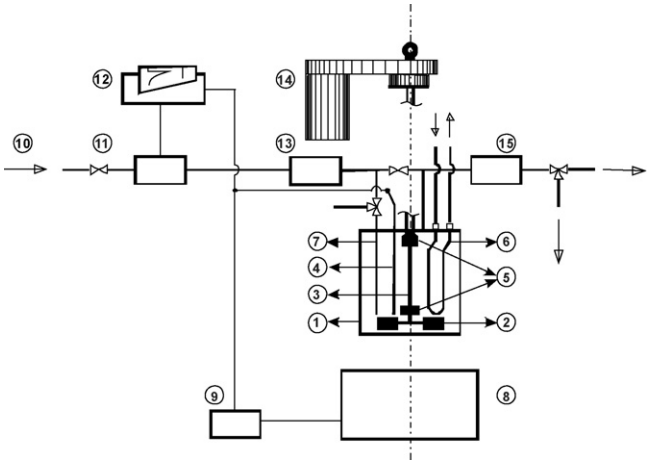

Fig. 1. Experimental setup: (1) reaction vessel; (2) impeller; (3) shaft stirrer; (4) temperature sensor; (5) CAC device; (6) cooling coil; (7) sampling valve and filter; (8) electrical heating furnace; (9) temperature controller; (10) gas inlet; (11) mass flow meter; (12) chart recorder; (13) pressure controller; (14) stirrer motor; (15) electronic pressure transducer.

Table 1
Experimental data and parameters used for estimation of the mass transfer effects on the hydrogenation rate

T (K)	P (bar)	$\Omega_H \times 10^{6}$[a] (mol cm^{-3} s^{-1})	$[k_b a_b]^{-1} \times 10^{2}$[b] (s)	$[a_c k_c]^{-1} \times 10^{1}$[c] (s)	$\frac{\Omega_H^{max} \times 10^2}{k_b a_b C_H^*}$	$\frac{\Omega_O^{max} \times 10^2}{k_c a_c C_O}$	$D_O^{eff} \times 10^{6}$[d] (cm^2 s^{-1})	$D_H^{eff} \times 10^{4}$[e] (cm^2 s^{-1})	$\Phi_H \times 10^{3}$[f]	$\Phi_O \times 10^{2}$[g]
398	3.7	4.3	3.7	4.0	5.9	0.6	1.2	5.5	0.4	1.1
443	6.5	14.6	3.5	2.9	2.0	1.5	1.8	7.4	1.0	4.4

$k_b a_b$, volumetric gas–liquid mass-transfer coefficient; $k_c a_c$, volumetric liquid–solid mass-transfer coefficient for methyl oleate; C_O, concentration of methyl oleate in bulk liquid phase; C_H^*, concentration of dissolved hydrogen in bulk liquid phase; Ω_H^{max}, maximum reaction rate of hydrogen; Ω_O^{max}, maximum reaction rate of methyl oleate; D_O^{eff}, effective intraparticle diffusion coefficient for methyl oleate; D_H^{eff}, effective intraparticle diffusion coefficient for hydrogen; Φ_H, Weisz and Prater module for hydrogen (dimensionless); Φ_O, Weisz and Prater module for methyl oleate (dimensionless).

[a] Experimental data at 1000 rpm.
[b] Experimental value obtained using the technique previously reported [19].
[c] Value calculated from ref. [29].
[d] Values calculated from correlation given by ref. [55].
[e] Values calculated from correlation given by ref. [55].
[f] Value calculated from ref. [31].
[g] Value calculated from correlation given by ref. [32].

2.3. Experimental procedure

The typical procedure was as follows: A precise amount of catalyst (8×10^{-2} g) was placed into the cup mounted on the upper part of the CAC device. Methyl oleate (40 g) was charged into the reactor, which was purged three times with nitrogen and then flushed with hydrogen at room temperature. Then, the reactor was pressurized with hydrogen and heated up to the reaction temperature. The catalyst was conditioned in situ and the liquid phase saturated with hydrogen under the reaction conditions. After 120 min, the reaction was allowed to start by suddenly imbedding the cup into the reaction mixture, as described elsewhere [19]. Zero time was taken just at that moment. Induction periods were not observed in any of the experiments. Samples of the reaction mixture were withdrawn at different time intervals, with on-line removing of the catalyst using a sinter metal filter. The reaction was stopped as soon as no detectable hydrogen consumption occurred.

2.4. Analytical method

The liquid samples were analyzed by gas-chromatography without *cis–trans* methyl oleate resolution. The GC analyses were performed on a gas chromatograph (Shimadzu GC-17AATF) equipped with a stainless steel column (2 m × 3.175 mm OD) packed with 15% DEGS-PS on GasChrom Z (80–100 mesh). Nitrogen was used as carrier gas (25 mL/min). The column was kept at a constant temperature, 453 K. The flame ionization detector (FID) and injector temperatures were 513 and 523 K, respectively. The concentrations of methyl oleate (O) and methyl estearate (S) in the reaction mixture were determined using methyl heptadecanoate (Aldrich, 99%) as internal standard.

2.5. Mass transport effects

Mass-transfer processes for hydrogen and FAMEs are often rate-determining steps (RDS) of three-phase hydrogenation systems [3,24–28]. Therefore, special care was taken to ensure that neither the gas–liquid, liquid–solid, nor intraparticle mass-transfer rates disguised the intrinsic kinetics. Table 1 shows the experimental data and parameters used for estimation of the mass transfer effects on the hydrogenation rate.

The effect of the hydrogen gas–liquid interfacial mass transfer on the hydrogenation rate was evaluated according to the technique reported in a previous work [19]. By varying the catalyst loading, the gas–liquid mass-transfer resistance was found to be less than 3.7×10^{-2} s. The ratio between the highest initial hydrogenation rate and the maximum interfacial transport rate of hydrogen was less than 5.9×10^{-2}, which suggests negligible gas–liquid interfacial mass-transfer limitations. The effects of hydrogen and methyl oleate mass transport from the bulk to the external catalyst surface were calculated from widely used correlations [29,30]. The values of the liquid–solid mass-transfer resistances were found to be within the 0.7–1.0 × 10^{-2} and 2.9–4.0 × 10^{-1} s ranges for hydrogen and methyl oleate, respectively. Thus, the corresponding values of the ratio between the highest initial hydrogenation rate and the maximum extraparticle mass-transfer rate were lower than 1.5×10^{-3} and 3.3×10^{-3}, respectively, which indicates negligible extraparticle mass-transfer limitations for both reactants. The intraparticle diffusion limitations were estimated from well-known criteria. The initial hydrogenation rate was found to be nearly first-order for the hydrogen and almost zero-order for the methyl oleate. Then, according to the Weisz and Prater analysis, the intraparticle resistance for hydrogen transport can be neglected if $\Phi_H \ll 1$ [31]. The criterion becomes $\Phi_O \ll 2$ for methyl oleate [32]. The values of the Weisz and Prater modules were found to be $\Phi_H < 1.0 \times 10^{-3}$ and $\Phi_O < 4.4 \times 10^{-2}$, which revealed negligible intraparticle mass-transfer limitations. Concluding, all these results indicate the absence of any mass-transfer limitations from the experimental data included in this study. Temperature gradients are also unlikely to occur because the reaction is moderately exothermic [3].

3. Adsorption models

Before further derivation of the kinetic equations describing the hydrogenation rate of methyl oleate, a general approach concerning adsorption models will be illustrated without expressing

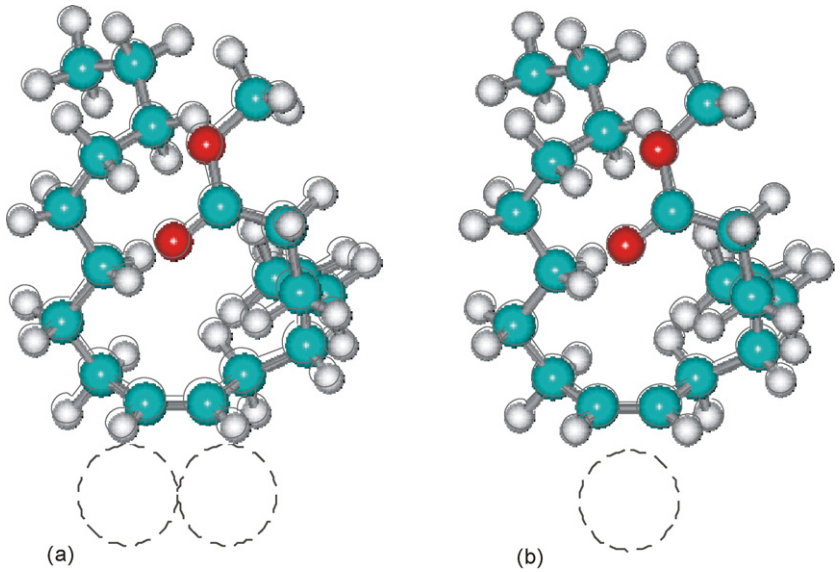

Fig. 2. Molecular structure of *cis*-methyl oleate, $C_{19}H_{36}O_2$. Schematic representation showing: (a) 2σ-adsorption mode and (b) π-adsorption mode.

opinion *a priori* on whether the adsorption between hydrogen and FAMEs is competitive or non-competitive. To formulate the surface site balance equations for hydrogen and FAMEs adsorption on the same type of ⊗-sites, it is assumed that the *i*-FAME molecule interacts with x_i metal atoms, being either 2 for adsorption involving a 2σ-complex or 1 for adsorption forming a π-complex (Fig. 2). It is also assumed that the adsorption of hydrogen can be non-dissociative or dissociative.

3.1. The general formulation

Understanding that FAME molecules are much larger than both the hydrogen molecule and the distance between neighbouring free-sites, it is assumed that the *i*-FAME molecule additionally covers s_i sites closely adjacent to the x_i sites on which it is justly adsorbed. The s_i sites are assumed to be inaccessible for the adsorption of another molecule of FAME due to steric hindrance but they are available for hydrogen adsorption. Concisely, it is postulated that the molecule of the *i*-FAME effectively covers $(x_i + s_i)$ surface sites. For a better understanding of what is mentioned above, see Fig. 3.

Admitting the distinction between occupied-sites (x_i) and covered-sites $(x_i + s_i)$, there are two forms of expressing the surface site balance equation

$$\sum x_i \Theta_i + \Theta_{H_{2\,/\,n}} + \Theta_{\otimes} = 1 \tag{1}$$

$$\sum (x_i + s_i)\Theta_i + \Theta^{U}_{H_{2\,/\,n}} + \Theta^{U}_{\otimes} = 1 \tag{2}$$

where the summation sign indicates the sum of all FAMEs, n is either 1 for non-dissociative adsorption of hydrogen or 2 for dissociative adsorption of hydrogen, and superscript U denotes uncovered by the FAME molecules, i.e., $\Theta^{U}_{H_{2\,/\,n}}$ and $\Theta^{U}_{\otimes}$ account the hydrogen and free-sites surface coverages remaining uncovered between the molecules of FAMEs, respectively. Since the

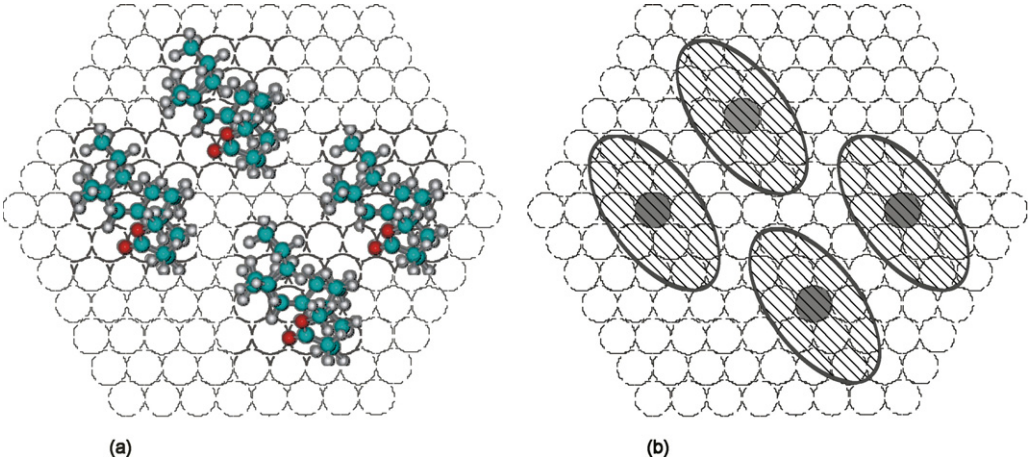

Fig. 3. Artist's view of adsorption of *cis*-methyl oleate on Ni(1 1 1) showing: (a) rough representation of a possible close-packed monolayer, the centres of the C9:10 double bounds have been arbitrarily placed on-top of Ni atoms; (b) schematic representation of occupied-sites (shaded regions) and covered-sites (dashed regions) by the adsorbed molecules of *cis*-methyl oleate; uncovered-sites between them.

s_i surface sites might be accessible for adsorption of the small molecules of hydrogen, $\Theta_{\otimes}$ is the fractional surface coverage of ⊗-sites available for hydrogen adsorption, but for FAMEs is $\Theta_{\otimes}^{U}$ only. Eq. (1) establishes the relationship to be fulfilled at the catalyst surface, whereas Eq. (2) accounts for the surface site inventory as observed from a top view as depicted in Fig. 3b.

Defining a parameter f as the ratio between the occupied-sites and covered-sites by the FAMEs

$$f = \frac{\sum x_i \Theta_i}{\sum (x_i + s_i)\, \Theta_i} \tag{3}$$

which decreases from 1 to small values at increasing molecular sizes, Eq. (2) can conveniently be rewritten as follows

$$\sum x_i \Theta_i + f(\Theta_{H_{2/n}}^{U} + \Theta_{\otimes}^{U}) = f \tag{4}$$

where the uncovered fractional surface coverages are governed by the following relationship

$$1 + f(\Theta_{H_{2/n}}^{U} + \Theta_{\otimes}^{U}) = f + \Theta_{H_{2/n}} + \Theta_{\otimes} \tag{5}$$

as obtained from Eqs. (1) and (4).

Assuming the quasi-equilibrium approximation for the adsorption of the species

$$\Theta_i = K_i C_i (\Theta_{\otimes}^{U})^{x_i} \tag{6}$$

$$\Theta_{H_{2/n}} = (K_H C_{H_2})^{1/n} \Theta_{\otimes} \tag{7}$$

and by substituting Eqs. (6) and (7) into Eqs. (4) and (5), we finally obtain

$$\sum x_i K_i C_i (\Theta_{\otimes}^{U})^{x_i} + f[1 + (K_H C_{H_2})^{1/n}]\Theta_{\otimes}^{U} = f \tag{8}$$

$$\Theta_{\otimes} = \frac{1 - f\{1 - [1 + (K_H C_{H_2})^{1/n}]\Theta_{\otimes}^{U}\}}{1 + (K_H C_{H_2})^{1/n}} \tag{9}$$

Eq. (8) expresses that the maximum surface coverage of FAMEs can only be the fraction f of total ⊗-sites. This relation certainly governs the free-sites surface coverage remaining uncovered between the molecules of FAMEs, and it has to be solved implicitly for $\Theta_{\otimes}^{U}$ unless $x_i = 1$ (π-adsorption). Eq. (9) completes the mathematical model by establishing the relationship between $\Theta_{\otimes}^{U}$ and $\Theta_{\otimes}$. It is right to think of Eqs. (8) and (9) as an advantageous frame to describe the surface site balance because the well-known equations for competitive and non-competitive adsorption regimes can be directly derived as asymptotic cases for f approaching its extreme values. This feature will be shown for $x_i = 1$ since explicit expressions are only feasible to be obtained for this common case.

3.2. Competitive and non-competitive adsorption models as asymptotic cases

Parameter f should have a value within the $0 < f \leq 1$ range. Hence, the following two asymptotic cases can be examined.

3.2.1. Case a: Competitive adsorption ($f = 1$)

From the physical meaning of parameter f, this special case describes a one-to-one correspondence between occupied-sites and covered-sites by the adsorbed molecules, as expected for small molecules. Solving Eqs. (8) and (9) for $f = 1$, it yields

$$\Theta_{\otimes}^{U} = \Theta_{\otimes} = \frac{1}{1 + (K_H C_{H_2})^{1/n} + \sum K_i C_i} \tag{10}$$

and, using this result, Eqs. (6) and (7) become

$$\Theta_i = \frac{K_i C_i}{1 + (K_H C_{H_2})^{1/n} + \sum K_i C_i} \tag{11}$$

$$\Theta_{H_{2/n}} = \frac{(K_H C_{H_2})^{1/n}}{1 + (K_H C_{H_2})^{1/n} + \sum K_i C_i} \tag{12}$$

which can be recognized as the expressions of FAMEs and hydrogen surface coverages which result from the competitive adsorption model.

3.2.2. Case b: Semi-competitive adsorption ($f \to 0$)

This special case suggests that the covered-sites are much more than those occupied-sites by the adsorbed organic species, as expected for molecules much larger than hydrogen. By letting $f \to 0$ in Eqs. (8) and (9), we obtain

$$\Theta_{\otimes}^{U} = \frac{f}{\sum K_i C_i} \tag{13}$$

$$\Theta_{\otimes} = \frac{1}{1 + (K_H C_{H_2})^{1/n}} \tag{14}$$

and, therefore, from Eqs. (6) and (7) we have the following expressions for the FAMEs and hydrogen surface coverages

$$\Theta_i = \frac{f K_i C_i}{\sum K_i C_i} \tag{15}$$

$$\Theta_{H_{2/n}} = \frac{(K_H C_{H_2})^{1/n}}{1 + (K_H C_{H_2})^{1/n}} \tag{16}$$

which are in agreement with the non-competitive adsorption model.

Thus, the cases of competitive and non-competitive adsorption were matched in a continuous form by varying parameter f from unity to a small but non-zero value, respectively. Accordingly, within the present mathematical framework, the description of semi-competitive regimes would be approachable by using intermediate values of parameter f. The usefulness of this approach will now be illustrated for the kinetic study of the liquid-phase hydrogenation of methyl oleate on Ni/α-Al_2O_3 catalyst.

4. Results and discussion

4.1. Reaction mechanism and kinetic models

The kinetic equations are derived assuming that: (i) there is only one type of ⊗-sites for the adsorption of hydrogen and FAMEs [17,33–36]; (ii) the hydrogen adsorption can be either non-dissociative [10,12,16] or dissociative [10,17,18,24,33–37]; (iii) FAMEs can adsorb in one of the following two ways: as a 2σ-complex interacting with two

neighboring nickel atoms ($x=2$) or as a π-complex involving a single nickel atom ($x=1$) [3,13]; (iv) no distinction is made for migration products because the double bound shifts only one position around the normal one of the methyl oleate C18 : $1\Delta_9^c$ [10]; (v) the methyl oleate (*cis*) and methyl elaidate (*trans*) are considered as a lumped species, named methyl oleate, without *cis–trans* distinction since the hydrogenation and adsorption rate constants are comparable for both geometrical isomers [10,16,17,38]; (vi) the hydrogenation of the double bound is explained on the bases of the Horiuti–Polanyi mechanism, involving a half-hydrogenated surface intermediate [3,10,13,17–19,33–35,39,40]; (vii) the fractional surface coverage by intermediate adsorbed species is negligible compared to those of bulk species [10,41–43]; (viii) the fractional surface coverage by the saturated compound (methyl estearate) is not neglected *a priori* [10,16]; (ix) parameter f does not depend on the temperature. We fully use a simplified mechanistic scheme because our main goal is only to exemplify the usefulness of the approach for analyzing different models based on competitive, non-competitive, and semi-competitive adsorption of the species, without undertaking the study of the *cis–trans* isomerization process.

The following equilibria and elementary steps are considered: adsorption of hydrogen and methyl oleate on the ⊗-sites (steps (S1) and (S2)); reversible reaction of the methyl oleate with adsorbed hydrogen yielding the half-hydrogenated surface intermediate SH (step (S3)), followed by an irreversible second addition of hydrogen (step (S4)) and fast desorption of the methyl estearate (step (S5)).

M3: DAH ($n=2$) with 2σ-adsorption ($x=2$) and first H-addition as RDS;
M4: AAH ($n=1$) with 2σ-adsorption ($x=2$) and first H-addition as RDS;
M5: DAH ($n=2$) with π-adsorption ($x=1$) and second H-addition as RDS;
M6: AAH ($n=1$) with π-adsorption ($x=1$) and second H-addition as RDS;
M7: DAH ($n=2$) with 2σ-adsorption ($x=2$) and second H-addition as RDS;
M8: AAH ($n=1$) with 2σ-adsorption ($x=2$) and second H-addition as RDS.

After some algebra using classical LHHW calculations, the methyl oleate hydrogenation rate can be described by the following rate equations:

For models *M1–M4*

$$\Omega_O = -k_{SH}(K_H C_{H_2})^{1/n} K_O C_O (\Theta_\otimes^U)^x \Theta_\otimes \quad (17)$$

For models *M5–M8*

$$\Omega_O = -k_1 K_{SH} K_H C_{H_2} K_O C_O (\Theta_\otimes^U)^x (\Theta_\otimes)^{2-x} \quad (18)$$

where $\Theta_\otimes^U$ and $\Theta_\otimes$ are governed by Eqs. (8) and (9).

As f approaches unity or small but not zero values, these full expressions properly simplify to the classical LHHW expressions for the extreme cases of competitive adsorption and non-competitive adsorption as summarized in the first and second columns of Table 2, respectively.

Elementary steps of the reaction pathway		Adsorption and rate constants
$H_2 + n(\otimes) \leftrightarrows n(\otimes)\text{-}H_{2/n}$	(S1)	K_H, (k_H and k_{-H})
$O + x(\otimes) \leftrightarrows (x\otimes)\text{-}O$	(S2)	K_O, (k_O and k_{-O})
$(x\otimes)\text{-}O + (\otimes)\text{-}H_{2/n} \leftrightarrows (\otimes)\text{-}SH + (2-n)(\otimes)\text{-}H + (n+x-2)(\otimes)$	(S3)	K_{SH}, (k_{SH} and k_{-SH})
$(\otimes)\text{-}SH + (\otimes)\text{-}H \rightarrow (x\otimes)\text{-}S + (2-x)(\otimes)$	(S4)	k_1
$(\otimes)\text{-}S \leftrightarrows S + x(\otimes)$	(S5)	K_S, (k_S and k_{-S})

where n is either 1 for non-dissociative adsorption of hydrogen or 2 for dissociative adsorption of hydrogen; x is either 1 for π-adsorption or 2 for σ-adsorption.

Further kinetic model assumptions are as follows: (x) the surface sites are uniform and homogeneously distributed [10,16,17,24]; (xi) the hydrogen adsorption is at equilibrium (step (S1)) [10,16–18,24,38]; (xii) the adsorption of FAMEs is assumed to be fast, which implies quasi-equilibrium for the adsorption of methyl oleate (step (S2)) [16,37,41,44,45]; (xiii) the first or second addition of hydrogen to the double bound can be RDS (steps (S3) or (S4)).

Depending on different combinations of adsorption modes and elementary RDS, eight kinetic models were formulated. The models are denoted as follows

M1: DAH ($n=2$) with π-adsorption ($x=1$) and first H-addition as RDS;
M2: AAH ($n=1$) with π-adsorption ($x=1$) and first H-addition as RDS;

4.2. Parameter estimation procedure

A reduction of the number of models to be tested was made because models *M2* and *M6* are identical for parameter estimation purposes. Then, seven models describing non-competitive, semi-competitive and competitive adsorption were subsequently evaluated by varying parameter f, and by performing the model discrimination using Fisher's test and further physical interpretation.

Non-linear regression analysis of experimental data was performed for the kinetic models. The residual sum of squares between experimental data and predictions was minimized by a modified Levenberg–Marquard algorithm combined with a procedure for solving non-linear least squares problems [46]. The numerical integration of the hydrogenation rate equations was performed using a Runge–Kutta (2,3) pair method [47]. The

Table 2
Hydrogenation rate equations for non-competitive and competitive adsorption as asymptotic cases of the full expressions given by Eqs. (8), (9), (17) and (18), Ω_O (mol cm^{-3} s^{-1})

Model	Asymptotic expressions of Ω_O for extreme values of f	
	$f \to 0$ (Non-competitive adsorption)	$f = 1$ (Competitive adsorption)
M1	$-\dfrac{fk_{SH}\sqrt{K_H C_{H_2}}K_O C_O}{(1+\sqrt{K_H C_{H_2}})(K_O C_O + K_S C_S)}$	$-\dfrac{k_{SH}\sqrt{K_H C_{H_2}}K_O C_O}{(1+\sqrt{K_H C_{H_2}} + K_O C_O + K_S C_S)^2}$
M2 = M6	$-\dfrac{fkK_H C_{H_2}K_O C_O}{(1+K_H C_{H_2})(K_O C_O + K_S C_S)}$ [a]	$-\dfrac{k_{SH}K_H C_{H_2}K_O C_O}{(1+K_H C_{H_2} + K_O C_O + K_S C_S)^2}$
M3	$-\dfrac{fk_{SH}\sqrt{K_H C_{H_2}}K_O C_O}{2(1+\sqrt{K_H C_{H_2}})(K_O C_O + K_S C_S)}$	$-k_{SH}\sqrt{K_H C_{H_2}}K_O C_O \Theta_\otimes^3$ where $2(K_O C_O + K_S C_S)\Theta_\otimes^2 + (1+\sqrt{K_H C_{H_2}})\Theta_\otimes = 1$
M4	$-\dfrac{fk_{SH}K_H C_{H_2}K_O C_O}{2(1+K_H C_{H_2})(K_O C_O + K_S C_S)}$	$-k_{SH}K_H C_{H_2}K_O C_O \Theta_\otimes^3$ where $2(K_O C_O + K_S C_S)\Theta_\otimes^2 + (1+K_H C_{H_2})\Theta_\otimes = 1$
M5	$-\dfrac{fk_1 K_{SH}K_H C_{H_2}K_O C_O}{(1+\sqrt{K_H C_{H_2}})(K_O C_O + K_S C_S)}$	$-\dfrac{k_1 K_{SH}K_H C_{H_2}K_O C_O}{(1+\sqrt{K_H C_{H_2}} + K_O C_O + K_S C_S)^2}$
M7	$-\dfrac{fk_1 K_{SH}K_H C_{H_2}K_O C_O}{2(K_O C_O + K_S C_S)}$	$-k_1 K_{SH}K_H C_{H_2}K_O C_O \Theta_\otimes^2$ where $2(K_O C_O + K_S C_S)\Theta_\otimes^2 + (1+\sqrt{K_H C_{H_2}})\Theta_\otimes = 1$
M8	$-\dfrac{fk_1 K_{SH}K_H C_{H_2}K_O C_O}{2(K_O C_O + K_S C_S)}$	$-k_1 K_{SH}K_H C_{H_2}K_O C_O \Theta_\otimes^2$ where $2(K_O C_O + K_S C_S)\Theta_\otimes^2 + (1+K_H C_{H_2})\Theta_\otimes = 1$

[a] $k = k_1 k_{SH}$ for model *M2* and $k = k_1 k_{SH}$ for model *M6*.

optimization of the kinetic parameters was achieved fitting the experimental data for all three pressures at the reference temperature of 413 K, followed by the estimation of the activation energies and adsorption heats according to the Arrhenius and Van't Hoff laws, respectively, in the whole temperature range

$$k(T) = k(T_r)\exp\left(-\frac{E}{RT'}\right) \tag{19}$$

$$K(T) = K(T_r)\exp\left(-\frac{\Delta H}{RT'}\right) \tag{20}$$

where T' is given by

$$\frac{1}{T'} = \frac{1}{T} - \frac{1}{T_r} \tag{21}$$

and T_r is the reference temperature.

Concerning the significance of the estimated parameters, the individual 95% confidence intervals have been calculated. The analysis of the significance of the overall regression and the goodness-of-fit were appraised based upon Fisher's test [48,49]

$$F_{calc} = \frac{\sum_{h=1}^{\upsilon}\sum_{k=1}^{\upsilon}\sigma^{hk}\sum_{i=1}^{n}C_{calc,ih}C_{calc,ik}/p}{\sum_{h=1}^{\upsilon}\sum_{k=1}^{\upsilon}\sigma^{hk}\sum_{i=1}^{n}(C_{obs,ih}-C_{calc,ih})(C_{obs,ik}-C_{calc,ik})/(n\upsilon-p)} \tag{22}$$

where $C_{obs,ij}$ and $C_{calc,ij}$ are the observed and calculated concentrations values for the ith FAME of the jth data point, respectively; σ^{hk} are the elements of the inverse of the error covariance matrix ($\upsilon \times \upsilon$), n represents the number of experimental data per FAME, υ is the number of FAMEs, and p is the number of adjusted parameters of the model. The regression was considered to be meaningful when the F_{calc} value was greater than the corresponding tabulated F-value. The highest F_{calc} value was taken as indicative of the best possible regression. The adequacy of the fitting was also checked examining the residual sum of square (SSQ) and the residual plots.

4.3. Discrimination of kinetic models

The optimization of the kinetic and adsorption constants was carried out by fitting methyl oleate concentration versus time data from 93 observations, in both time and temperature domains. A first optimization was performed at the reference temperature of 413 K, followed by a second optimization in the temperature domain. After estimation of $k_1 k_{SH}$ or $k_1 K_{SH}$, K_H, K_O and K_S at 413 K, the data at all temperatures were simultaneously fitted by means of the reparameterization given by Eqs. (19)–(20). The K_S/K_O ratio was found to be ranging from 10^{-2} to 10^{-3} for all the kinetic models. In order to reduce the number of the parameter to be estimated, the adsorption of the methyl estearate was then assumed to be negligible, and consequently the adsorption constant K_S ruled out. This is in agreement with the observed preferential adsorption of the unsaturated compounds over the saturated ones [4,9,17,20–22,33–35,50], and the fast desorption rate of the methyl estearate [24,38,50].

Table 3 summarizes the SSQ and F_{calc} values obtained by non-linear regression analysis for the seven kinetic models tested with f ranging from 0.025 (non-competitive adsorption) to 1 (competitive adsorption), at 413 K. Models *M1* and *M3* provide the worst quality of the kinetic description since they exhibit

Table 3
Residual sum of squares (SSQ) and *F*-test values (F_{calc}) in the *f* domain for the kinetic models and the set of experimental data at 413 K, and hydrogen pressure of 3.7, 5.1 and 6.5 bar

Model		Adsorption regime										
		Non-competitive		Semi-competitive								Competitive
	f	0.025	0.1	0.2	0.3	0.4	0.5	0.6	0.7	0.8	0.9	1.0
M1	SSQ × 10^7	2.92	1.10	1.02	1.13	1.16	1.21	1.03	1.22	1.21	1.22	1.17
	F_{calc}	1466.1	3788.6	4066.3	3689.6	3582.7	3421.4	4033.1	3414.7	3443.1	3410.4	3528.6
M2 = M6	SSQ × 10^7	1.28	0.45	0.35	0.35	0.35	0.35	0.34	0.34	0.34	0.34	0.34
	F_{calc}	3345.0	9342.7	11934.1	11851.9	11898.8	12025.7	12108.8	12065.7	12070.3	12065.6	12067.0
M3	SSQ × 10^7	4.11	3.39	3.33	1.04	1.05	1.05	1.07	2.53	2.58	2.59	2.49
	F_{calc}	1051.4	1251.8	1269.2	4007.7	3972.3	3952.9	3900.9	1664.6	1631.9	1627.6	1694.8
M4	SSQ × 10^7	6.32	1.21	0.87	0.45	0.47	0.46	0.48	0.47	0.47	0.35	0.35
	F_{calc}	691.7	3497.7	4838.7	9355.6	8920.1	9011.9	8704.1	8951.9	8796.1	11891.6	11892.0
M5	SSQ × 10^7	0.96	0.41	0.35	0.35	0.33	0.34	0.37	0.33	0.33	0.33	0.33
	F_{calc}	4432.7	10025.4	11867.6	11962.0	12370.9	12207.9	12282.0	12386.4	12385.7	12390.2	12384.3
M7	SSQ × 10^7	0.85	0.34	0.34	0.34	0.34	0.33	0.34	0.33	0.33	0.33	0.34
	F_{calc}	4997.1	12101.8	12178.6	12086.7	12086.4	12339.5	12370.1	12367.4	12369.3	12366.9	12269.2
M8	SSQ × 10^7	2.73	0.46	0.49	0.35	0.35	0.35	0.36	0.36	0.37	0.35	0.34
	F_{calc}	1571.2	9015.1	8542.6	11743.5	11743.5	11696.8	11608.5	11641.0	11304.3	11905.1	12058.5

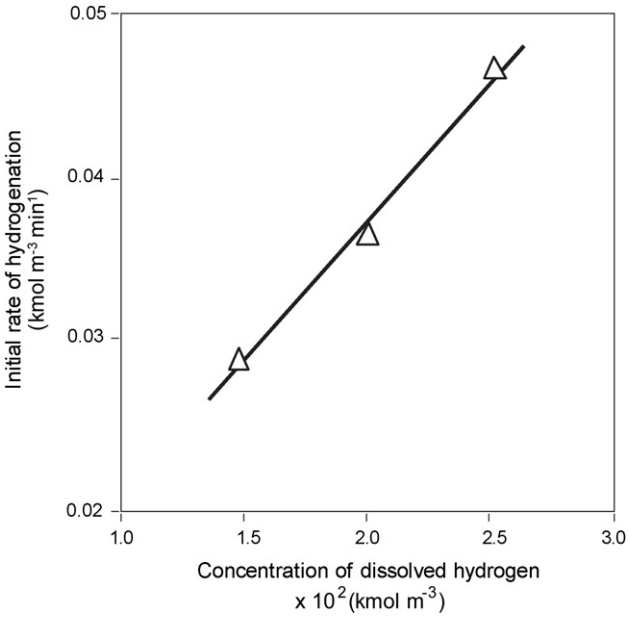

Fig. 4. Initial rate of hydrogenation as a function of the dissolved hydrogen concentration at 413 K and 3.7, 5.1 and 6.5 bar. Catalyst loading: 0.2 wt% with respect to methyl oleate. Stirring rate: 1000 rpm.

the lowest F_{calc} values, whichever the *f* value. The primary difference between both models and the other ones is a half-order dependence on the reaction rate, which is in disagreement with the first-order one often found in the liquid-phase hydrogenation of FOs and FAMEs [4,10,16,17,24,38,50,51]. Fig. 4 shows an almost linear dependence of the initial rate of hydrogenation with the concentration of dissolved hydrogen corroborating that the hydrogen reaction order is close to one within the range of studied pressures. Therefore, models *M1* and *M3* were then promptly excluded for further consideration. The remaining five models were subsequently evaluated. All these models for the non-competitive adsorption regime ($f \rightarrow 0.05$) were found to be unable to describe our experimental data, but the data fitting resulted acceptable for *f* values ranging from 0.10–0.30 to 1.00, depending on the kinetic model. Unfortunately, the SSQ and F_{calc} values are almost equal within this broad range of *f* values; therefore, we cannot statistically distinguish between the models for semi-competitive and competitive regimes.

An attempt to discriminate between the five models led us to make a rough estimate of the amount of surface sites covered by the methyl oleate molecule, and to compare the resulting value with the maximum admissible ones for each model according to the corresponding *f* and *s* values. While several surface science groups have studied the adsorption of short-chain unsaturated compounds on transition-metal surfaces, the adsorption of long-chain unsaturated compounds has received considerably less attention. Hence, the amount of sites covered by the methyl oleate molecule adsorbed on Ni surfaces is still certainly unknown. As far as we know, for compounds analogous to methyl oleate, optimized structures and adsorption energies have only been reported to *cis*-4-decene on different Pd clusters [13]. By simple inspection, it is plausible that the *cis*-4-decene can cover up to five or six sites on the Pd surface. Although

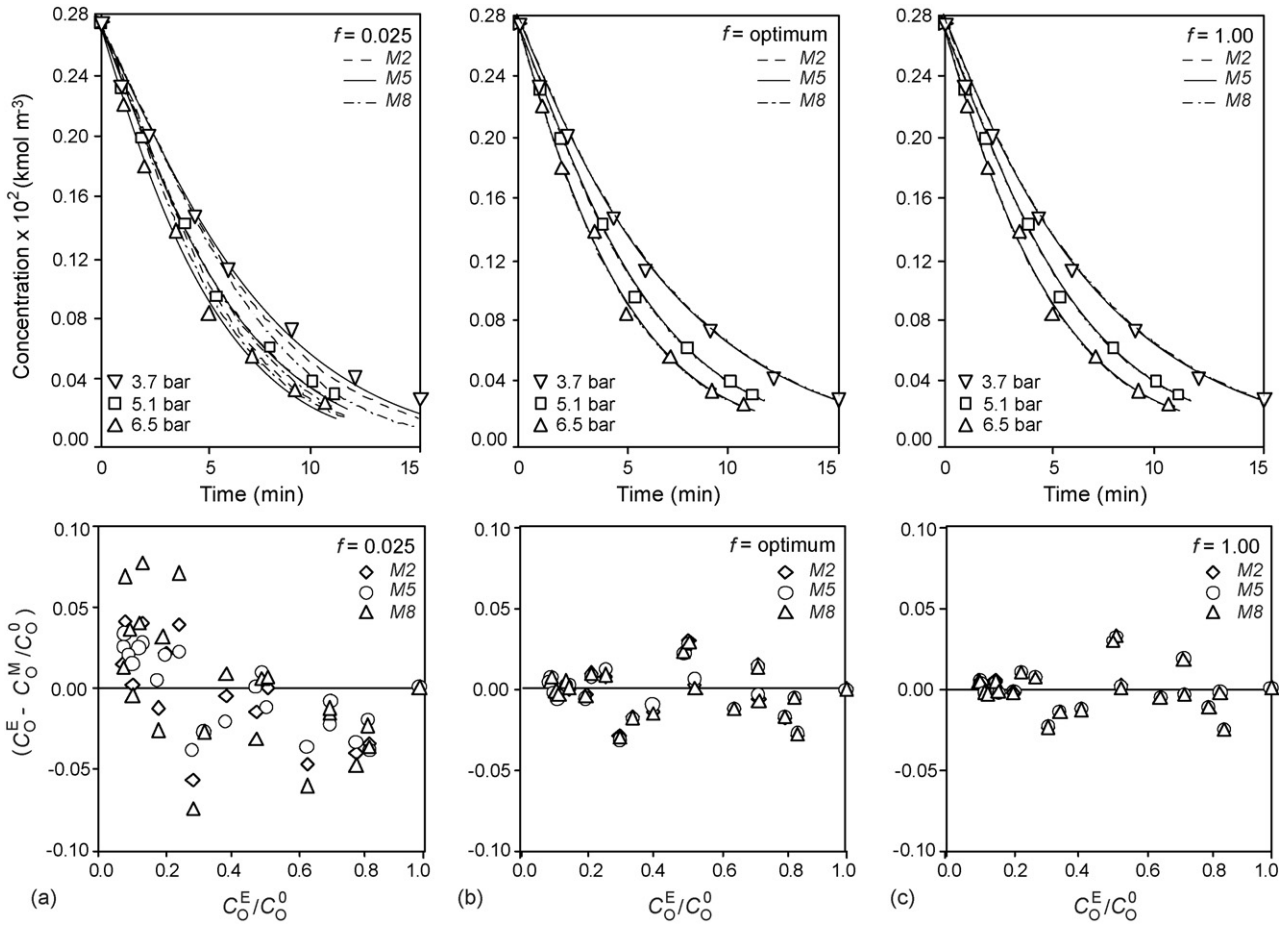

Fig. 5. Experimental and predicted composition profiles in the time domain (upper figure), and residuals between model predictions and experimental data in the conversion domain (lower figure) for models *M2*, *M5* and *M8,* at 413 K, and 3.7, 5.1 and 6.5 bar. (a) Non-competitive adsorption: $f = 0.025$. (b) Semi-competitive adsorption: $f = 0.15$, 0.16, and 0.29 (optimised values); (c) competitive adsorption: $f = 1.00$.

there are differences in the interaction of olefins with Pd and Ni, a larger surface coverage appears to be plausible for the *cis*-methyl oleate molecule due to its large molecular size. Detailed molecular modeling would support some knowledge of the structure involved in the adsorption of methyl oleate. This is, however, not within the scope of the present contribution. We estimated a value by assuming a primitive structure (optimized estimation using AM1 method), and inferred that the surface covered by the methyl oleate would be around 45–50 Å^2, which is nearly equivalent to seven or eight Ni atoms on a Ni(1 1 1) surface, as schematically depicted in Fig. 3. These estimated values are in good agreement with those reported for *cis*-4-decene due to the larger molecular size of the *cis*-methyl oleate.

An inspection of the *SSQ* and F_{calc} values reported in Table 3 reveals that the *M4* and *M7* models are not entirely consistent because they suggest coverages up to 2.2 ($f \approx 0.9$ and $x = 2$) and 20 ($f \approx 0.1$ and $x = 2$) sites, respectively, which are far away from admissible values. Consequently, models *M4* and *M7* were also excluded from the inventory of models. On the contrary, models *M2*, *M5* and *M8* gave indications that the adsorbed molecule of methyl oleate could cover around seven surface sites, as expected. Indeed, the estimates are 7.14 ($f \approx 0.14$ and $x = 1$), 6.67 ($f \approx 0.15$ and $x = 1$) and 6.90 ($f \approx 0.29$ and $x = 2$) sites, respectively. According to the view presented here, all three models appear to be the only valid candidates. Unfortunately, the semi-competitive models do not further improvement of the experimental data fitting in comparison with the extreme competitive models. Fig. 5 shows the experimental and predicted composition profiles in the time domain (upper figure), and the residuals between the predictions of the models and experimental data in the conversion domain (lower figure), at 413 K, and 3.7, 5.1 and 6.5 bar. The non-uniform and broad bands of residuals certainly confirm the inadequacy of the extreme non-competitive models, but the more uniform and narrow bands of residuals corroborate that semi-competitive and extreme competitive models are not decidedly different from each other. Nevertheless, since the geometric restrictions of the methyl oleate molecule can be more satisfactorily explained by the semi-competitive models than by the competitive ones, the semi-competitive models are slightly favored.

Some additional differences between the models with both rival adsorption modes could be recognized from the estimated parameters in the temperature domain, which are summarized in Table 4. Slightly higher and lower adsorption constants for hydrogen and methyl oleate, respectively, as well as higher kinetic constants, are observed for the semi-competitive mod-

Table 4
Fitted parameter values for models *M2*, *M5* and *M8* with 95% confidence limits, in the range of $398 \leq T \leq 443$ K and $3.7 \leq P_{H_2} \leq 6.5$ bar

Model	$k \times 10^4$[a] (mol L^{-1} s^{-1})	K_O[a] (mol^{-1} L)	K_H[a] (mol^{-1} L)	E (kJ mol^{-1})	$-\Delta H_O$ (kJ mol^{-1})	$-\Delta H_H$ (kJ mol^{-1})
M2						
$f = 0.025$	7.96 ± 0.06	30.64 ± 0.29	26.32 ± 0.67	62.08 ± 0.70	24.78 ± 0.75	43.63 ± 0.79
f = 0.14	*10.43 ± 0.07*	*28.21 ± 0.51*	*11.01 ± 0.22*	*68.39 ± 0.85*	*11.14 ± 0.70*	*50.60 ± 0.76*
$f = 1.00$	3.51 ± 0.03	85.30 ± 0.47	10.06 ± 0.15	69.08 ± 0.82	9.17 ± 0.68	52.15 ± 0.83
M5						
$f = 0.025$	6.07 ± 0.08	25.38 ± 0.36	71.77 ± 0.68	74.48 ± 0.71	10.60 ± 0.69	74.99 ± 0.79
f = 0.16	5.98 ± 0.04	49.44 ± 0.43	19.17 ± 0.31	85.17 ± 0.73	10.13 ± 0.64	77.70 ± 0.73
$f = 1.00$	4.05 ± 0.02	104.06 ± 0.64	10.59 ± 0.18	90.24 ± 1.02	8.32 ± 0.39	81.05 ± 0.83
M8						
$f = 0.025$	15.26 ± 0.14	18.57 ± 0.71	25.14 ± 0.66	64.24 ± 0.73	20.47 ± 0.79	44.03 ± 0.72
f = 0.29	*10.22 ± 0.09*	*26.15 ± 0.85*	*13.34 ± 0.19*	*72.85 ± 0.78*	*16.82 ± 0.72*	*50.94 ± 0.79*
$f = 1.00$	3.91 ± 0.03	70.08 ± 0.62	12.03 ± 0.31	72.54 ± 2.03	14.07 ± 0.56	52.02 ± 0.91

[a] Value at the reference temperature of 413 K. The italicized values correspond to the optimal *f* values.

els in comparison with the competitive ones, while the activation energies and adsorption heats remain almost constant whichever the value of *f*. The calculated model parameters and confidence intervals reveal no significant differences between models *M2* and *M8* around the optimized values of parameter *f*, except for model *M5*. The estimated adsorption heats for methyl oleate ($-\Delta H_O$) are around 10 kJ mol^{-1} for models *M2* and *M5*, and 16 kJ mol^{-1} for model *M8*. The heat of vapor-phase adsorption of methyl oleate on Ni/α-Al_2O_3 has been measured to be 75 ± 6 kJ mol^{-1} [33–35], but there are no available data for liquid-phase adsorption. Although the liquid-phase process can differ from the vapor-phase process, the difference between the corresponding adsorption heats is presumed to be around the heat of vaporization, which is 81.5 kJ mol^{-1} for the *cis*-methyl oleate [52]. From these data, the heat of liquid-phase adsorption is expected to be quite a small value, which is in agreement with previous kinetic studies considering the temperature effect on the adsorption constants of unsaturated triglycerides negligible [38,53]. Thus, models *M2* and *M5* are somewhat favored. Estimates of the heat of adsorption of hydrogen ($-\Delta H_H$) are around 50 kJ mol^{-1} for models *M2* and *M8*, and about 77.7 kJ mol^{-1} for model *M5*. The heat of hydrogen adsorption on Ni/α-Al_2O_3 has previously been measured to be 70.7 kJ mol^{-1} using the H_2/D_2 exchange [36]. This value is also consistent with the heat of hydrogen adsorption on Pd/α-Al_2O_3 measured calorimetrically, which was reported to be around 73 kJ mol^{-1} [54]. Therefore, when comparing the values of the heats of adsorption, model *M5* is the preferred one.

With the data summarized above, and at this stage of understanding, the most convincing of the seven models is model *M5*. This model explains the hydrogenation kinetics on the basis of dissociative adsorption of hydrogen ($n = 2$), methyl oleate molecule interacting with a single atom of Ni ($x = 1$), and second insertion of hydrogen to the half-hydrogenated intermediate as the more likely RDS. Even though estimates from model *M5* for semi-competitive and competitive adsorption modes are statistically indistinguishable, we consider the model approaching semi-competitive adsorption as more realistic because besides exhibiting physically reasonable values for the estimated parameters ($E = 85.17$ kJ mol^{-1}; $-\Delta H_O = 10.13$ kJ mol^{-1}, and $-\Delta H_H = 77.70$ kJ mol^{-1}), it suggests that the adsorbed molecule of methyl oleate could cover up to almost seven surface sites, which is in close agreement with the rough value calculated from geometrical considerations.

5. Conclusions

The kinetic modeling of the liquid-phase hydrogenation of methyl oleate over Ni/α-Al_2O_3 was performed on the basis of elementary step mechanisms involving different regimes of competition between hydrogen and methyl oleate. Based upon plausible mechanisms, kinetic models were derived by accounting different regimes of competition between hydrogen and methyl oleate for adsorption on the same type of surface sites. Admitting the distinction between occupied-sites and covered-sites by the large molecule of methyl oleate, a rigorous proposal was made to link the seemingly separate kinetic models corresponding to the extreme modes of competitive and non-competitive adsorption, without having to draw the common distinction between two types of surface sites. The proposed approach gives a workable way to survey intermediate (semi-competitive) competition regimes.

Kinetic experiments in the absence of mass-transport limitation were carried out for $398 \leq T \leq 443$ K and $3.7 \leq P_{H_2} \leq 6.5$ bar, using a catalyst loading of 0.2 wt% and a stirring rate of 1000 rpm. General rate equations were formulated without expressing opinion *a priori* on whether the adsorption between hydrogen and FAMEs is competitive or non-competitive. Then, typical LHHW rate equations for both extreme adsorption regimes were straightforwardly derived as special cases. A statistical analysis of regression using our experimental data shows the inadequacy of the models approaching the extreme non-competitive adsorption regime. The mechanistic model featuring dissociative adsorption of hydrogen, molecule of methyl oleate interacting with a single atom of Ni, and second insertion of hydrogen as RDS, proved to be the best candidate to describe the data satisfactorily with physically reasonable parameters. Statistical results do not allow a definite discrimination between rival models with competitive and semi-competitive adsorption. As a distinctive feature, the model considering semi-competitive

adsorption appears to be more realistic than the competitive one because it gives additional insight into the amount of surface sites that can be covered by the adsorbed molecule of methyl oleate. It may be said that the results presented in this work support the usefulness of this approach to deal with intermediate regimes of adsorption, but further work should be done in order to demonstrate its effectiveness to perform kinetic studies on other hydrogenation systems. Therefore, future studies, especially on the liquid-phase hydrogenation of substituted cyclic olefins, such as monoterpenes, are already being planned.

Acknowledgments

The authors wish to express their gratitude to the Agencia Nacional de Promoción Científica y Tecnológica (ANPCyT), to Consejo Nacional de Investigaciones Científicas y Técnicas (CONICET), and to Universidad Nacional del Litoral (UNL) of Argentina, for the financial support granted to this contribution.

References

[1] I.V. Deliy, N.V. Maksimchuk, R. Psaro, N. Ravasio, V. Dal Santo, S. Recchia, E.A. Paukshtis, A.V. Golovin, V.A. Semikolenov, Appl. Catal. A: Gen. 279 (2005) 99–107.
[2] B. Nohair, C. Especel, G. Lafaye, P. Marécot, L. Chién, J. Hoagn, Barbier, J. Mol. Catal. A: Gen. 229 (2005) 117–126.
[3] J.W. Veldsink, M.J. Bouma, N.H. Schöön, A.A.C.M. Beenackers, Catal. Rev. Sci. Eng. 39 (1997) 253–318.
[4] J.W.E. Coenen, Ind. Eng. Chem. Fundam. 25 (1986) 43–52.
[5] A.J. Wright, A. Wong, L.L. Diosady, Food Res. Int. 36 (2003) 1069–1072.
[6] J.P. Szybist, A.L. Boehman, J.D. Taylor, R.L. McCormick, Fuel Process. Technol. 86 (2005) 1109–1126.
[7] N. Ravasio, F. Zaccheria, M. Gargano, S. Recchia, A. Fasi, N. Poli, R. Psaro, Appl. Catal. A: Gen. 233 (2002) 1–6.
[8] M. Izadifar, M. Zolghadri Jahromi, J. Food Eng. 78 (2007) 1–8.
[9] B. Fillion, B.I. Morsi, Ind. Eng. Chem. Res. 39 (2000) 2157–2168.
[10] G.H. Jonker, J.W. Veldsink, A.A.C.M. Beenackers, Ind. Eng. Chem. Res. 36 (1997) 1567–1579.
[11] G.H. Jonker, J.W. Veldsink, A.A.C.M. Beenackers, Ind. Eng. Chem. Res. 37 (1998) 4646–4656.
[12] M.T. Rodrigo, L. Daza, S. Mendioroz, Appl. Catal. A: Gen. 88 (1992) 101–114.
[13] M.B. Fernández, G.M. Tonetto, G.H. Crapiste, M.L. ferreira, D.E. Damianai, J. Mol. Catal. A: Gen. 237 (2005) 67–79.
[14] J.-P. Mikkola, H. Vainio, T. Salmi, R. Sjöholm, T. Ollonqvist, J. Väyrynen, Appl. Catal. A: Gen. 196 (2000) 143–155.
[15] H. Backman, A.K. Neyestanaki, D. Yu, Murzin, J. Catal. 233 (2005) 109–118.
[16] G. Gut, J. Kosinka, A. Prabucki, A. Schuerch, Chem. Eng. Sci. 34 (1979) 1051–1056.
[17] R.J. Grau, A.E. Cassano, M.A. Baltanás, Ind. Eng. Chem. Process Des. Dev. 25 (1986) 722–729.
[18] K. Hashimoto, K. Katsuhiko, S. Nagata, JACOS 48 (1971) 291–295.
[19] R.J. Grau, A.E. Cassano, M.A. Baltanás, Ind. Eng. Chem. Res. 26 (1987) 18–22.
[20] R.J. Grau, A.E. Cassano, H.A. Irazoqui, Chem. Eng. Commun. 64 (1988) 47–65.
[21] R.J. Grau, A.E. Cassano, M.A. Baltanás, Chem. Eng. Sci. 43 (1988) 1125–1132.
[22] R.J. Grau, A.E. Cassano, M.A. Baltanás, Catal. Rev. Sci. Eng. 30 (1988) 1–48.
[23] R.J. Grau, A.E. Cassano, M.A. Baltanás, J. Am. Oil Chem. Soc. 67 (1990) 226–229.
[24] J. Marangozis, O.B. Keramidas, G. Paparisvas, Ind. Eng. Chem. Process Des. Dev. 16 (1977) 361–369.
[25] L. Bern, M. Hell, N.H. Schöön, J. Am. Oil. Chem. Soc. 52 (1975) 182–187.
[26] L. Bern, M. Hell, N.H. Schöön, J. Am. Oil. Chem. Soc. 52 (1975) 391–394.
[27] A.A. Susu, Appl. Catal. 4 (1982) 307–320.
[28] A.H. Chen, D.D. McIntire, P. Gibson, J.E. Covey, J. Am. Oil Chem. Soc. 60 (1983) 1326–1330.
[29] P.L.T. Brian, H.B. Hales, AIChE J. 15 (1969) 419–425.
[30] A.A.C.M. Beenackers, W.P.M. Van Swaaij, Chem. Eng. Sci. 48 (1993) 3109–3139.
[31] P.B. Weisz, C.D. Prater, Adv. Catal. 6 (1954) 143–196.
[32] D.E. Mears, J. Catal. 20 (1971) 127–131.
[33] J.-O. Lidefelt, J. Magnusson, N.-H. Schoon, J. Am. Oil. Chem. Soc. 60 (1983) 600–602.
[34] J.-O. Lidefelt, J. Magnusson, N.-H. Schoon, J. Am. Oil. Chem. Soc. 60 (1983) 603–607.
[35] J.-O. Lidefelt, J. Magnusson, N.-H. Schoon, J. Am. Oil. Chem. Soc. 60 (1983) 608–613.
[36] J. Magnusson, Ind. Eng. Chem. Res. 26 (1987) 874–877.
[37] A.A. Susu, A.F. Ogunye, C.O. Onyegbado, J. Appl. Chem. Biotechnol. 28 (1978) 823–833.
[38] B. Fillion, B.I. Morsi, K.R. Heier, R.M. Machado, Ind. Eng. Chem. Res. 41 (2002) 697–709.
[39] J. Horiutti, M. Polanyi, Trans. Faraday Soc. 30 (1934) 1164–1172.
[40] H.J. Dutton, C.R. Scholfield, E. Selke, W.K. Rohwedder, J. Catal. 10 (1968) 316–327.
[41] J.J. Zwicky, G. Gut, Chem. Eng. Sci. 33 (1978) 1363–1369.
[42] G.H. Graaf, J.G. Winkelman, E.J. Stamhuis, A.A.C.M. Beenackers, Chem. Eng. Sci. 43 (1988) 2161–2168.
[43] G.H. Graaf, E.J. Stamhuis, A.A.C.M. Beenackers, Chem. Eng. Sci. 43 (1988) 3185–3195.
[44] P. Van der Plank, J. Catal. 26 (1972) 42–50.
[45] P. Van der Plank, B.G. Linsen, H.J. Van den Berg, Proceedings of the Fifth (2nd Int.) Symposium on Chemical Reaction Engineering, Amsterdam, 1972, pp. B6–B21.
[46] D.W. Marquardt, J. Soc. Ind. Appl. Math. 11 (1963) 431–441.
[47] R.W. Brankin, I. Gladwell, L.F. Shampine, RKSUITE: A Suite of Runge Kutta Codes for the Initial Value Problem for ODES, Softreport 91-1, Mathematics Department, Southern Methodist University, Dallas, Texas, 1991.
[48] G.F. Froment, L.H. Hosten, in: J.R. Anderson, M. Boudart (Eds.), Catalysis Science and Technology, vol. 2, Sringer-Verlag, Berlin, 1981, pp. 97–170.
[49] G.F. Froment, in: G.F. Froment, K.B. Bischoff (Eds.), Chemical Reactor Analysis and Design, second ed., John Wiley & Sons, New York, 1990.
[50] K. Tsuto, P. Harriott, K.B. Bischoff, Ind. Eng. Chem. Fundam. 17 (1978) 199–205.
[51] G.C.M. Colen, G. Van Duijn, H.J. Van Oostern, Appl. Catal. 43 (1988) 339–350.
[52] R.C. Weast, M.J. Astle, W.H. Beyer, CRC Handbook of Chemistry and Physics, 67th ed., Boca Raton, Florida, 1986.
[53] E. Santacesaria, P. Parella, M. snm Di Serio, G. Borelli, Appl. Catal. A: Gen. 116 (1994) 269–294.
[54] P. Chou, M.A. Vannice, J. Catal. 104 (1987) 1–16.
[55] C.N. Satterfield, C.K. Colton, E.H. Pitcher, AIChE J. 19 (1973) 628–635.